AXIAL FLOW TRANSITIONS IN A CONFINED VORTEX

T.W. Mattner, P.N. Joubert and M.S. Chong.
Department of Mechanical and Manufacturing Engineering
University of Melbourne, Parkville VIC 3052, Australia.

ABSTRACT

Annular regions of reversed axial flow have been observed in highly swirled confined vortices. The aim of the present paper is to examine transition to this regime with increase in swirl. A spiral disturbance, similar to vortex breakdown, caused transition from jet-like to wake-like axial velocity profiles. As the swirl was increased, a second transition to a W shaped axial velocity profile occurred. This gradually developed with further increase in swirl until an annulus of reversed axial flow was observed.

INTRODUCTION

Extensive regions of reversed axial flow are not uncommon in confined vortex flows. Nuttal (1953) identified three modes of axial flow: positive axial flow everywhere (regime I), reversed axial flow at the centre of the vortex (regime II) and an annulus of reversed axial flow (regime III). Transition from one regime to the next was achieved by an increase in swirl intensity, although Binnie (1957) later found that end-walls were necessary to achieve regime III. Several explanations for this behaviour have been proposed in the literature, however, it is difficult to form general conclusions because of the variety of apparatus, boundary conditions and flow parameters used.

Transition from regime I to regime II can occur as a result of vortex breakdown. Harvey (1962) investigated vortex breakdown in a guide vane driven apparatus with a flared tube and a uniform, screened outlet. At low swirl, a uni-directional vortex (regime I) was obtained, but as the swirl intensity increased, a breakdown appeared downstream. The breakdown moved upstream with further increase in the swirl intensity, eventually disappearing to leave a vortex with a core region of reversed axial velocity which filled the entire length of the tube (regime II). He did not, however, report any observation of regime III.

Similar behaviour was reported by Escudier & Keller (1985) who measured the flow field in a model swirl stabilised combustion chamber. They observed regime II flow and, in addition, found that the introduction of a contraction at the outlet had a severe effect on the upstream flow in this case. They therefore deduced that the post-breakdown, regime II flow was subcritical (i.e. capable of sustaining infinitesimal waves which propagate against the flow). A contraction caused the post-breakdown, regime II flow to revert to a uni-directional flow and, if the contraction was sufficiently strong, the axial velocity profile consisted of a central jet with a minima in the annular region surrounding the jet, as if the flow were approaching regime III.

Mattner *et al.* (1996) observed regime III axial flow at high swirl in a jet-driven confined vortex apparatus which included an orifice outlet. However, high turbulence levels and large asymmetry prevented detailed observations of the transition from regime I to regime III. Mattner *et al.* (1998) improved this apparatus by replacing the tangential jets with guide vanes and introducing honeycombs and screens which reduced the turbulence level by an order of magnitude. They observed two transitions: the first from a jet-like axial velocity (with maximum axial velocity near the vortex centre) to a wake-like axial velocity (with minimum axial velocity near the centre), and the second to a W shaped profile (with an axial velocity minima in an annulus surrounding the centre). The minimum axial velocity continued to decrease with further increase in swirl un-

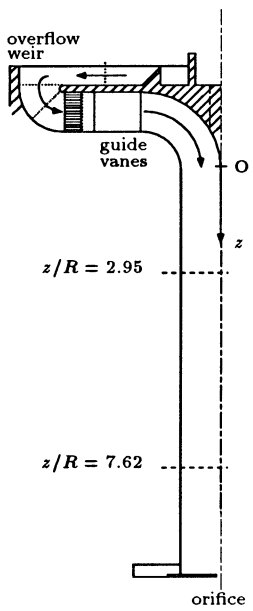

Figure 1: Radial cross-section of the apparatus.

til an annulus of reversed axial flow (regime III) was established.

Mattner *et al.* (1998) found it difficult to reliably reproduce the transitional flows on separate occasions and were therefore unable to obtain detailed measurements in these regimes. There are at least three possible practical reasons for this variation: air entrapment during start-up, temperature (and hence, fluid property) variation and corrosion build-up on the walls of the apparatus. The purpose of this investigation, therefore, is to confirm the previous experimental results and examine the transition between flow regimes using a refined apparatus and experimental technique.

EXPERIMENTAL APPARATUS & TECHNIQUES

The geometry of the apparatus is identical to that used by Mattner *et al.* (1998) and is shown schematically in figure 1. Sixteen guide vanes or blades are arranged symmetrically about the axis of symmetry of the pipe. A centrepiece installed above the vanes guides the fluid smoothly into the working section. A series of screens and honeycomb upstream of the vanes reduces the turbulence and ensures the incoming flow is initially radial. Swirl was controlled by the blade angle β defined as the angle between the blade chord and a radial line from the axis of symmetry and shown in figure 2. An overflow weir fixed the height of the free surface and an orifice of diameter 14.25 mm at the outlet to the working section fixed the flow rate. Exhausted fluid is returned to a reservoir from which it is pumped back up to the upper side of the centrepiece. The working section consisted of a straight perspex pipe of inner radius

β (deg)	Ω	Re
19	0.79	4859
23	0.99	4915
25	1.09	4896
26	1.15	4868
29	1.32	4896
44	2.57	4906
45	2.70	4915
46	2.83	4915
69	21.6	4953

Table 1: Flow parameters.

$R = 86.1$ mm and length $L = 902$ mm. Axial position was referenced to an origin located at the beginning of the straight section and was measured positive in the direction of the mean axial flow.

Following the experiments of Mattner *et al.* (1998), the apparatus was disassembled and the centrepiece, blades and entry to the working section repainted to reduce the corrosion build-up. A heat exchanger was installed in the reservoir which allowed the equilibrium temperature to be maintained independent of environmental fluctuations to an accuracy of $\pm$ 0.2 deg. C. The apparatus was filled from below to expel the maximum amount of air from the system. The system was allowed 15 hrs to achieve thermal equilibrium and all measurements were completed without restarting or any adjustments being made.

The volume flow rate for each level of swirl was determined by measuring the time interval to collect a mass of fluid in a bucket. A Thermo Systems (TSI) 9100-7 two component laser Doppler velocimetry system was used to measure the azimuthal and axial velocities, denoted by V and W respectively. Frequency shifting was used to resolve flow reversals and reduce fringe bias. TSI IFA550 counter type processors were used to process the Doppler signal. Raw data was permanently stored and statistics calculated using inter-arrival time weighting (sample & hold) for lower data rates while controlled sampling techniques were used when data storage became excessive at higher data rates.

RESULTS & DISCUSSION

The volume flow rate $Q = 5.25 \times 10^{-4}$ m^{3}s^{-1} varied by less than $\pm 1.2\%$ over the entire range of swirl. Asymmetry in the pipe wall boundary layers at zero swirl prevented a precise determination of the flow rate from velocity measurements, however, ensemble averaged profiles were within $\pm 2\%$ while individual profiles were within $\pm 5\%$ of the true value. The pipe Reynolds number was defined as $Re = 2W_b R/\nu$ where $W_b = Q/\pi R^2$ (ie. the bulk axial velocity) and ν the kinematic viscosity. Variation of this parameter due to temperature and hence viscosity fluctuation was less then 0.5% compared with fluctuations of up to 5% in Mattner *et al.* (1998).

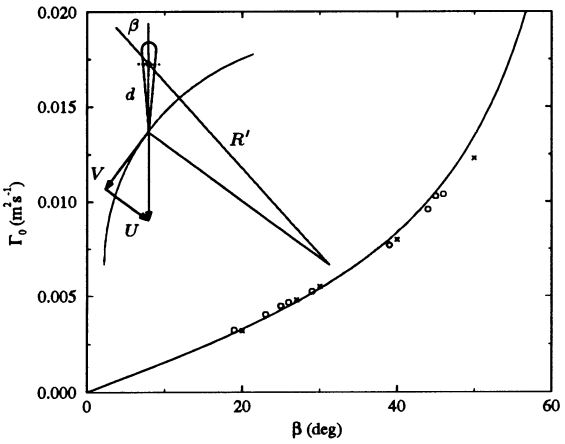

Figure 2: Equation (1) compared with Γ_0 estimated from: present data o; Mattner *et al.* (1998) ×.

Assuming that the flow at the trailing edge of a guide vane is parallel to its chord and a uniform radial velocity U, Escudier (1988) suggests that the maximum circulation Γ_0 imparted to the flow is given by

$$\Gamma_0 = \frac{Q}{H} \frac{\sin\beta}{\cos\beta - d/R'} \qquad (1)$$

where H is the vane span, d the distance from the vane shaft to its trailing edge and R' the distance from the vane shaft to the axis of symmetry and are shown in the inset of figure 2. For the present apparatus $H = 85.5$ mm, $d = 73.0$ mm and $R' = 252$ mm. Equation (1) is shown in figure 2 plotted versus the blade angle, together with the maximum circulation estimated from circulation distributions measured in the pipe. Taking into consideration the uncertainty of β ($\pm 0.5°$), equation (1) provides a good (within 5%) estimate of the maximum circulation for $\beta < 40°$. At larger β, equation (1) and the data diverge since:

1. Equation (1) indicates that $\Gamma_0 \to \infty$ as $\cos\beta \to d/R'$ and the assumptions upon which it is based must, therefore, eventually fail (e.g. by separation).
2. It becomes increasingly difficult to estimate Γ_0 from the experimental data for large β as there is no plateau in the circulation profiles and the outer flow becomes turbulent.

Despite these limitations, equation (1) is often used to calculate a swirl parameter, presently defined as $\Omega = \Gamma_0/2RW_b$ and calculated in table 1.

Mean axial and azimuthal velocity profiles and turbulence statistics were measured at nine equi-spaced stations along the pipe, from $z/R = 2.95$ to $z/R = 7.62$. This range, shown in figure 1, was determined by the travel limitations of the traverse. In all the velocity profile diagrams, the tube walls are represented by the lines bounding the profiles on either side. The aspect ratio is correct and the orientation consistent with figure 1, that is, with z positive down the page in the direction of the mean axial flow.

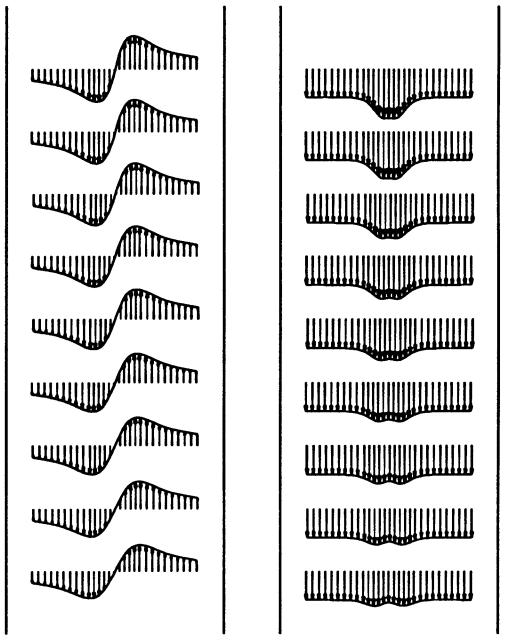

(a) V (b) W

Figure 3: $\beta = 23°$.

For $\beta \leq 23°$ the flow appears laminar and steady. Velocity profiles are similar in form to those observed by Faler & Leibovich (1978) and are shown for $\beta = 23°$ in figure 3. The peak velocities slowly decay with streamwise distance due to viscous diffusion. A sudden increase in β by 1°–2° leads to transient, almost axisymmetric structures such as those shown in figure 4. For $25° < \beta < 30°$ these disturbances develop into an asymmetric, unsteady, spiral pattern, similar to that shown in figure 5, which settles to an equilibrium position in the working section.

Figures 6–7 show two attempts to measure the flow with the spiral disturbance present. In the vicinity of the disturbance and further downstream, convergence histories show a very slow fluctuation. In practice, it was not feasible to extend the sample time in order to accommodate this slow fluctuation as the total running time became excessive and corrosion damage commenced. Detailed measurements (ie. increased resolution in the z direction) in the vicinity of the disturbance have therefore not been pursued. Nevertheless, these measurements show the sharp transition from jet-like to wake-like axial flow and almost stagnant flow in the vicinity of the disturbance. This behaviour is consistent with most descriptions of vortex breakdown. The equilibrium position of the disturbance moves upstream as

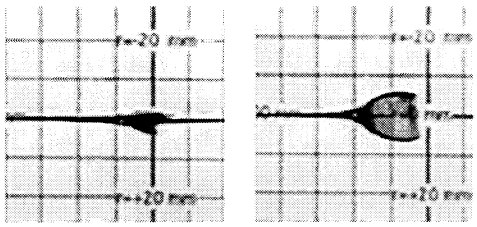

(a) $\Delta t = 0.00$ s (b) $\Delta t = 7.44$ s

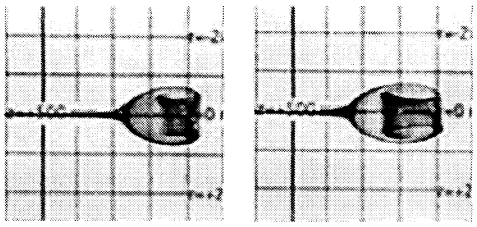

(c) $\Delta t = 12.6$ s (d) $\Delta t = 16.7$ s

Figure 4: Transient behaviour. Note that z is positive left to right.

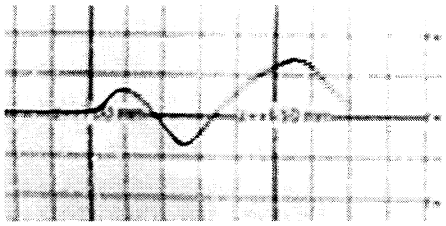

Figure 5: Ultimate behaviour. Note that z is positive left to right.

β is increased. The flow outside the core region appears undisturbed over the range of z measured. The axial flow remains uni-directional.

Figure 8 shows the centreline axial velocity plotted versus the axial distance. Closed symbols are extracted from local parabolic curve fits of the radial profiles while the open symbols are measurements at the nominal pipe centre. These will be slightly different, as the centre of the vortex rarely coincides exactly with this nominal position (variation of up to $0.02R$). Considering the comments in the previous paragraph, figure 8(a) shows reasonable agreement between the data. The centreline axial velocity does not show monotonic behaviour beyond the disturbance but appears to exhibit significant axial gradients. The centreline axial velocity profile in figure 8(b) (open symbols) shows several oscillations downstream of the disturbance, although it is difficult to determine if this is an actual feature of the flow due to the amount of scatter present and the unsatisfactory agreement between the two data sets.

Poorly converged data are to be expected in the

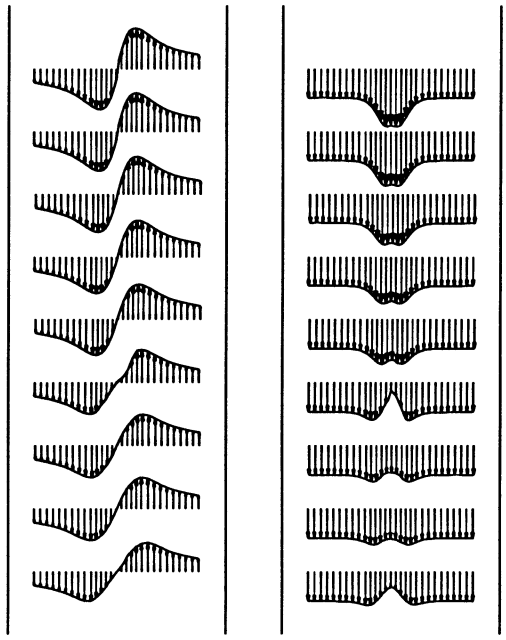

(a) V (b) W

Figure 6: $\beta = 26°$.

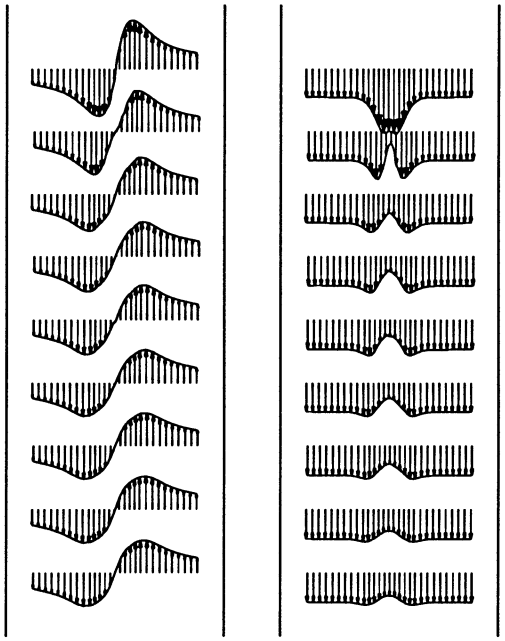

(a) V (b) W

Figure 7: $\beta = 29°$.

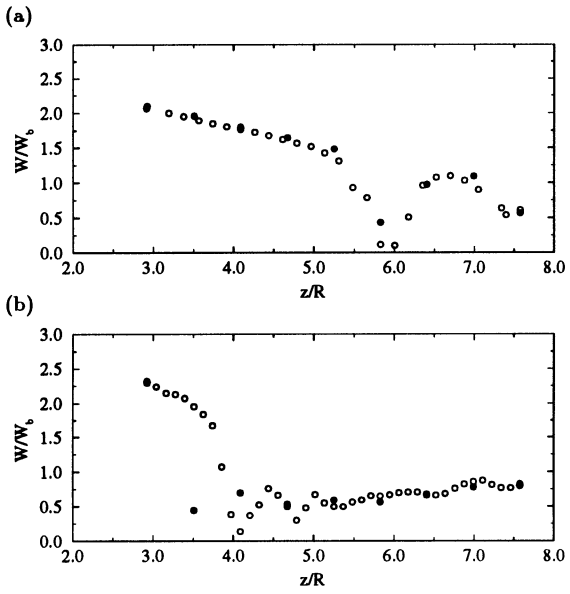

Figure 8: Mean centreline axial velocity for (a) $\beta = 26°$ and (b) $\beta = 29°$: • extracted from radial profiles; o measured at nominal pipe centre.

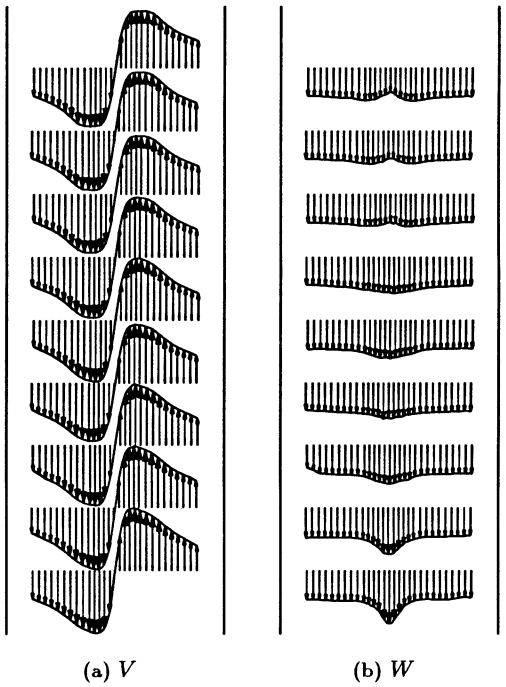

Figure 9: $\beta = 44°$.

vicinity of the disturbance where the axial gradients are large and its position fluctuates slowly. Faler & Leibovich (1978) encountered a similar problem when they mapped the internal structure of a bubble type vortex breakdown. They solved it by sampling only when the nose of the bubble was at a predetermined position. The present case may be more sensitive since there is no external forcing or tripping (such as the external adverse pressure gradient applied by Faler & Leibovich, 1978) and the disturbance location would then be affected only by the minor fluctuations present in the flow. If there were significant axial gradients in the mean velocity field downstream of the disturbance and if this flow field also fluctuated in position with the disturbance, then there would be a consistent explanation for the difficulty in achieving well converged results in the downstream flow. This question will need to be resolved by the use of conditional sampling, scanning or instantaneous flow field measurement techniques.

As β was increased further, the disturbance disappeared from view in the entry section of the apparatus leaving a turbulent vortex core in its wake. For $\beta \leq 44°$ there is a gradual recovery from a wake-like axial velocity profile to a jet-like profile with axial distance. The flow remains uni-directional which contrasts with the behaviour observed by Harvey (1962) but is consistent with the effect of a mild contraction on subcritical, post-breakdown flow noted by Escudier & Keller (1985). Figure 9 shows the behaviour at $\beta = 44°$.

The second transition to W shaped axial velocity profiles occurred quite suddenly between $\beta = 44°$ and $\beta = 45°$. Note that there is no evidence of W shaped profiles anywhere in the measurement domain in figure 9 but that this behaviour can be observed throughout the measurement domain in figure 10. In contrast to the first transition, which was quite localised, the second transition appears to be of a global nature. Further increase in β gradually decreases the minimum mean axial velocity and eventually leads to an annulus of reversed axial flow (regime III). This regime is shown at $\beta = 69°$ in figure 11 where it should be noted that the vector length scale has been reduced by 0.28 in comparison to previous figures to accommodate the large increase in the peak velocity magnitude. It is difficult to discern the annulus of negative axial velocity in these diagrams due to the dominance of the central velocity peak. These profiles are similar to those observed by Mattner *et al.* (1996) in a jet-driven, free surface vortex at high swirl. This suggests that regime III is not strongly dependent on the swirl generation device and is not due to possible separation on the guide vanes at large β. The axial velocity profiles in figure 10 are similar to those observed by Escudier & Keller (1985) in subcritical, post-breakdown flow in the presence of a strong contraction. This suggests that regime III flow arises from the introduction of a severe contraction (in this case an orifice) into subcritical, post-breakdown flow.

Upon careful inspection of the axial velocity profiles close to the walls in the downstream half of the measurement domain in figures 9 and 10, small depar-

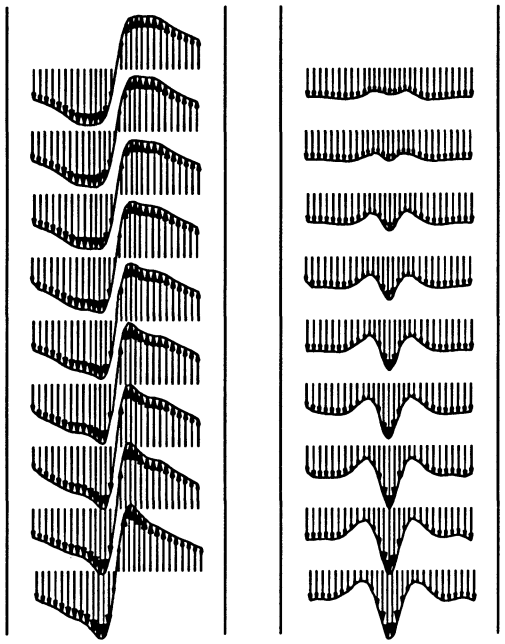

(a) V (b) W

Figure 10: $\beta = 45°$.

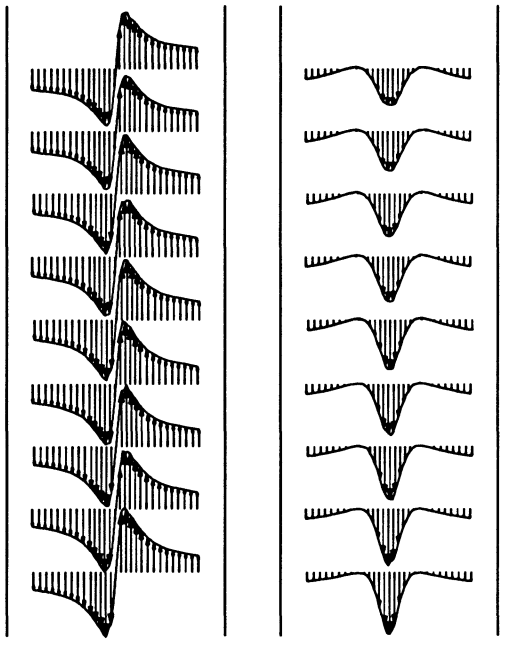

(a) V (b) W

Figure 11: $\beta = 69°$. Note that the vector length scale has been reduced by a factor 0.28 with respect to previous figures.

tures in uniformity of the axial velocity can be detected. These are associated with peaks in the rms velocities. Dye introduced upstream of the screens and honeycomb close to the outer wall has a streaky structure in the working section. Close to the downstream end of the apparatus, these structures periodically lift away from the wall, toward the centre of the vortex. These effects move upstream with increasing β until the entire flow (not just the core) becomes turbulent. These observations give the impression that laminar to turbulent boundary layer transition has commenced on the pipe walls.

CONCLUSION

Two transitions occur as β is increased in the present apparatus. The first, which occurs around $\beta = 25°$–$29°$, is characterised by a localised disturbance, consistent with spiral vortex breakdown, and a sharp transition from jet-like to wake-like axial velocity profiles. Straightforward, single point, time averaged measurements are not well suited to this transitional flow. The second transition to a W shaped axial velocity profile occurs throughout the measurement domain between $\beta = 44°$ and $45°$. Further increase in β causes this profile to gradually develop an annulus of reversed axial flow (regime III).

REFERENCES

Binnie, A.M., 1969, "Experiments on the slow swirling flow of a viscous liquid through a tube", *Quart. J. Mech. and Appl. Math.*, **3**, pp. 276–290.

Escudier, M.P. & Keller, J.J., 1985, "Recirculation in swirling flow: A manifestation of vortex breakdown", *A.I.A.A. Journal*, **23(1)**, pp. 111–116.

Escudier, M.P., 1988, "Vortex breakdown: Observations and explanations", *Prog. Aerospace Sci.*, **25**, pp. 189–229.

Faler, J.H., & Leibovich, S., 1978, "An experimental map of the internal structure of a vortex breakdown", *J. Fluid Mech.* , **86**, pp. 313–335.

Harvey, J.K., 1962, "Some observations of the vortex breakdown phenomenon", *J. Fluid Mech.*, **14**, pp. 585–592.

Mattner, T.W., Joubert, P.N. & Chong, M.S., 1996, "Investigation of the effect of downstream boundary conditions on a confined vortex flow", *First Australian conference on laser diagnostics in fluid mechanics*, University of Sydney, Sydney, Australia, pp. 180–185.

Mattner, T.W., Joubert, P.N. & Chong, M.S., 1998, "Axial flow regimes in a confined vortex", *13th Australasian Fluid Mechanics Conference*, Monash University, Melbourne, Australia, pp. 773–776.

Nuttal, J.B., 1953, "Axial flow in a vortex", *Nature*, **172**.